

Cosolute partitioning in polymer networks: Effects of flexibility and volume transitions

Won Kyu Kim,^{1,*} Arturo Moncho-Jordá,^{2,3} Rafael Roa,¹ Matej Kanduč,¹ and Joachim Dzubiella^{1,4,†}

¹*Institut für Weiche Materie und Funktionale Materialien,
Helmholtz-Zentrum Berlin, Hahn-Meitner-Platz 1, 14109 Berlin, Germany*

²*Departamento de Física Aplicada, Facultad de Ciencias,
Universidad de Granada, Avenida Fuente Nueva S/N, 18071 Granada, Spain*

³*Instituto Carlos I de Física Teórica y Computacional, Facultad de Ciencias,
Universidad de Granada, Avenida Fuente Nueva S/N, 18071 Granada, Spain*

⁴*Institut für Physik, Humboldt-Universität zu Berlin, Newtonstr. 15, 12489 Berlin, Germany*

We study the partitioning of cosolute particles in a thin film of a semi-flexible polymer network by a combination of coarse-grained (implicit-solvent) stochastic dynamics simulations and mean-field theory. We focus on a wide range of solvent qualities and cosolute–network interactions for selected polymer flexibilities. Our investigated ensemble (isothermal-isobaric) allows the network to undergo a volume transition from extended to collapsed state while the cosolutes can distribute in bulk and network, correspondingly. We find a rich topology of equilibrium states of the network and transitions between them, qualitatively depending on solvent quality, polymer flexibility, and cosolute–network interactions. In particular, we find a novel ‘cosolute-induced’ collapsed state, where strongly attractive cosolutes bridge network monomers albeit the latter interact mutually repulsive. Finally, the cosolutes’ global partitioning ‘landscape’, computed as a function of solvent quality and cosolute–network interactions, exhibits very different topologies depending on polymer flexibility. The simulation results are supported by theoretical predictions obtained with a two-component mean-field approximation for the Helmholtz free energy that considers the chain elasticity and the particle interactions in terms of a virial expansion. Our findings have implications on the interpretation of transport processes and permeability in hydrogel films, as realized in filtration or macromolecular carrier systems.

I. INTRODUCTION

Polymer networks such as microgels or hydrogels are integral components of modern soft functional material design. Important applications revolve around filtration, macromolecular carrier particles, functional coatings, sensors, and nanoreactors. [1–10] In all these systems the uptake, storage, and release of active agents and cosolutes (e.g., reactants, pollutants, ligands, drugs) are decisive processes, which have to be controlled and programmed to the material. The gels in these applications often form film-like layers [11, 12], shells, and membranes that modulate the permeation [13, 14] and separation of the cosolutes by their wide range of controllable physicochemical behavior. A fundamental property describing the permeation and sorption of cosolutes to polymer networks on the most global level is the partitioning

$$\mathcal{K} = c_c^{\text{in}}/c_c^{\text{out}}, \quad (1)$$

which is a ratio of cosolute concentrations inside and outside (in the bulk reservoir) of the gel [15]. Equilibrium partitioning is one of the two key ingredients to the *permeability* of hydrogels that eventually defines the degree of mass transport through the networks [16–18].

One notable physical property that distinguishes gels from ordinary polymeric solutions is the additional

inter-connectivity that cross-links individual polymer molecules. This higher level complexity yields an intriguing nature of the material that is liquid-like and also solid-like [19], which renders a well known transition phenomenon: Most hydrogels undergo a sharp reversible structural transition from swollen states to collapsed states [20–26]. This volume transition is a reversible function of the temperature [12, 27], or more general, solvent quality, but can also be triggered for some polymers by several environmental stimuli, such as pH, salinity [4], and, importantly in our context, the addition of co-solvents or co-solutes [28–31]. The responsiveness close to the volume transition enables a facilitated control of the gel structure and permeability, eventually bearing a number of applications in the realm of so-called stimuli-responsive, ‘smart’ polymer materials [4, 32].

Hence, many relevant and intertwined phenomena come into play for the partitioning of cosolutes into gels, such as network topology and heterogeneity, size exclusion, as well as attractive interactions such as van der Waals, hydrophobic and electrostatic interactions, strongly depending on the chemical nature of polymers, solvents, and cosolutes [33–37]. In responsive polymer materials, as referenced above, the presence and adsorption of cosolutes can lead to swelling or shrinking or even induce a volume transition of the network. Hence, in general the detailed mechanisms of partitioning in polymer networks can be expected to be utterly complex as they result from a subtle interplay of non-bonded interactions, network constraints, conformations, and their

* wonkyu.kim@helmholtz-berlin.de

† joachim.dzubiella@helmholtz-berlin.de

transitions on multiple scales. Therefore, little is known yet about the quantitative behavior of cosolute partitioning that can be raised during the swelling–collapse transition of the gels in contact with a reservoir of the cosolutes, despite the elaborate development of theories [19, 38–40] and simulations [41–58] for pure gel systems (no cosolutes included) over the past decades. Noteworthy exceptions are recent simulation works that study cosolute permeation of hollow nanogels [58] or the non-specific effects of charged solutes (mostly salt) and their electrostatic couplings in polyelectrolyte network gels [46–50, 52–57, 59, 60].

In this work, we build a minimalistic model system to study the partitioning of cosolute particles in a thin film of a semi-flexible polymer network by a combination of coarse-grained stochastic dynamics simulations and mean-field theory. We perform a systematic study focusing on effects of varying solvent qualities (from good to bad), specific cosolute–network interactions (from repulsive to highly attractive) as well as polymer flexibilities. We work in an isothermal-isobaric ensemble in order to include also the effects of network swelling, shrinking, and the volume transition, coupled to the equilibrium partitioning of the cosolutes from a reservoir. To start as simple as possible, we construct a coarse-grained gel consisting of a regular cubic network [44, 45, 61–64] of flexible or semi-flexible chains in the presence of cosolutes which are simply of monomer size, and we employ inter- and intra-particle interactions in terms of the generic Lennard-Jones (LJ) pair potentials, which can be easily tuned from repulsion to high attraction. Despite the minimalistic features of our model, we find very rich structural and partitioning topologies, which we summarize in state–diagrams in the solvent-quality–interaction space. A large influence of polymer flexibility, in terms of the gel volume response, transition order and sharpness, on the partitioning is observed. Our mean-field theory is fully consistent with the simulations and provides a theoretical interpretation of the complex coupled partitioning and network volume (transition) behavior.

II. METHODS

A. Simulation model

In our simulation model we consider a film of a cubic polymer network in implicit solvent and explicit cosolutes, where monomers, linkers, and cosolutes are represented by simple beads. For the polymers we employ a bead–spring model with the intra-chain Hamiltonian (in units of thermal energy, $k_B T \equiv 1/\beta$) as

$$U_i^B = k_s(r_{i,i+1} - \sigma)^2 + k_b(\theta_{i-1,i,i+1} - \theta_0)^2. \quad (2)$$

The first term is the harmonic bond potential with respect to the segmental bond distance $r_{i,i+1} = |\mathbf{r}_{i+1} - \mathbf{r}_i|$, with the spring constant $k_s = 80 k_B T / \sigma^2$ and the equilibrium bond length σ . The latter sets the length scale

of our system. The second term is a harmonic bending potential with respect to the internal angle $\theta_{i-1,i,i+1}$ of two adjacent segmental vectors $\mathbf{r}_{i+1} - \mathbf{r}_i$ and $\mathbf{r}_i - \mathbf{r}_{i-1}$, with a rigidity constant k_b . This potential we use to tune the network flexibility. Here, we choose the equilibrium angle $\theta_0 = 180^\circ$ [47, 50] to avoid additional complexity of introducing torsional potentials. With k_b we can interpolate between flexible chains, $k_b = 0$, to semi-flexible ones with k_b in the range of several $k_B T$, and finally very stiff networks for $k_b \gg k_B T$. For the cross-links we define cross-linking beads that are bonded analogously as described in eq (2) but in three perpendicular directions in order to establish a regular cubic network in 3D. Hence, a cross-linking bead has six neighbors, unless it is a surface bead in the thin film having only five neighbors. We do not consider an angular potential involving the cross-linkers [47].

In addition to the intra-bead potentials, all network beads and cosolute particles are subject to the Lennard-Jones (LJ) potential:

$$U_{ij}^{\text{LJ}} = 4\epsilon_{ij} \left[\left(\frac{\sigma_{ij}}{r_{ij}} \right)^{12} - \left(\frac{\sigma_{ij}}{r_{ij}} \right)^6 \right], \quad (3)$$

where σ_{ij} is the interaction size, and the parameter ϵ_{ij} (in units of $k_B T$) is the interaction energy parameter for $i, j = n, c$, that is, network and cosolute particles, respectively. For network monomers, $i, j = n$, we also refer to it ϵ_{nn} as the solvent quality parameter as it tunes from a perfect ideal polymer behavior ($\epsilon_{nn} = 0$) to a good solvent ($0 < \beta\epsilon_{nn} < 0.3$), passing the θ -solvent ($\beta\epsilon_{nn} = 0.3$, where the second virial coefficient for the LJ interaction vanishes) to a bad solvent ($\beta\epsilon_{nn} > 0.3$) [30, 58]. The parameter ϵ_{nc} refers to the cosolute coupling to the polymers, which also will be tuned from the ideal behavior to very attractive interactions. Furthermore, we fix the cosolute–cosolute interaction to a generic value $\epsilon_{cc} = 0.1 k_B T$, that ensures simple repulsion between the cosolute particles and avoids unwanted aggregation between them. For simplicity we keep $\sigma_{ij} \equiv \sigma$ for all the beads.

The thin film of a cubic network is initially located in the middle of the simulation box in a stretched form, periodically repeated in x - and y -directions, while in z -direction it is finite and in touch with a finite reservoir (see Figure 1 and Figure S1 in SI). The network film consists of 6 layers (in the xy plane) of 5×5 cross-linker beads, where every cross-linker is connected linearly by 4 beads so that the inter-cross-linker length (contour length) is $l = 5\sigma$. With that, there are 425 chains and 150 cross-linkers with total network particle number $N_n = 1850$, and the fraction of the cross-linker beads yields 8.1%. We perform simulations spanning a wide range of the rigidity constant, k_b , and the interaction parameters, ϵ_{ij} , and investigate how the system (with or without cosolutes) is affected by these parameters. In the systems including cosolutes we add $N_c = 576$ cosolute particles, amounting to an initial concentration

of $c_c \approx 0.012\sigma^{-3}$. The resulting packing fraction is $\phi_c = \pi\sigma^3 c_c/6 \approx 0.0064$. We thus work in the high dilution limit of cosolutes in the reservoirs.

B. Simulation protocol

We employ the LAMMPS software [65] with the stochastic Langevin integrator in an anisotropic NpT ensemble. The iteration time step $\delta\tau = 10^{-3}\tau$ defines the time unit $\tau = \sqrt{m\sigma^2/k_B T}$. The friction coefficient γ is chosen to have the momentum relaxation time $\tau_\gamma = m/\gamma = \tau$, so that the free cosolute motion becomes diffusive after 10^3 time steps. To maintain fixed pressure we use the Berendsen anisotropic barostat [66]. The pressure relaxation time is also chosen to be $\tau_p = \tau$. The simulation box is initially set to have the lengths $L_x = L_y = 25\sigma$ and the longitudinal length $L_z = 75\sigma$, with periodic boundary conditions in all three Cartesian directions. The long box length L_z is kept fixed, while L_x and L_y vary according to NpT ensembles with given particle number $N = N_n + N_c = 2426$, pressure $p_x = p_y = p$, and temperature T . In that way, the hydrogel is allowed to self-consistently sample its equilibrium volume and aspect ratio, given the prescribed interactions. As the hydrogel is connected to a (finite) reservoir of cosolutes, the cosolutes can always equilibrate their partitioning between the reservoir and the gel. The value of the lateral pressure is chosen to be $p = 6.5853 \times 10^{-4} k_B T / \sigma^3 \approx 1$ bar. The simulations are typically run up to $4 \times 10^6 \delta\tau = 4000\tau$ and we analyze the data in the last 20% of the production runs.

As a first illustration, Figure 1 shows snapshots of three representative equilibrium states of the network film conformations. When the network chains are sufficiently stiff and the network monomers are essentially repulsive ($\epsilon_{nn} = 0.1 k_B T$), as shown in Figure 1(a), the network structure is in a swollen state, i.e., in a good solvent. On the other hand, the swollen state is disfavored by large attractions between the network monomers, that eventually result in a collapsed state as shown in Figure 1(c), i.e., in a bad solvent. Figure 1(b) shows a semi-flexible network system close to its collapse transition point.

C. Models of flexible and semi-flexible networks

In most of the paper, we will focus on two network types that we coin ‘flexible’ and ‘semi-flexible’ and shall relate (as far as our minimal model allows) to representative polymers that are widely used in experiments. The first polymer could be based on a simple low-molecular mass monomer like ethylene glycol. It is known that the persistence length l_p of a polyethylene glycol (PEG) chain is $l_p \approx 0.38$ nm [67, 68]. In our coarse-grained chain model this would correspond roughly to a bead (monomer) size σ . Therefore, we focus on the limiting $k_b = 0$ case for our model flexible net-

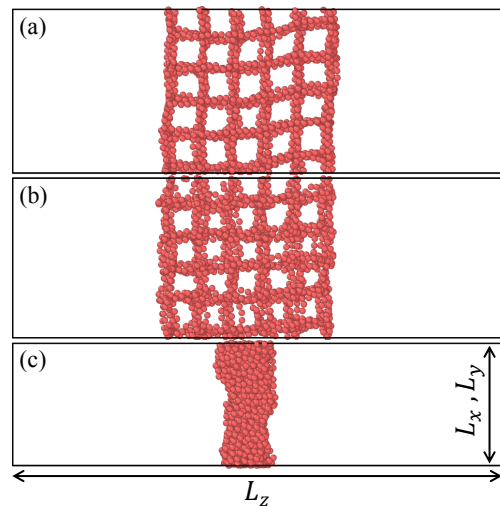


FIG. 1. Snapshots of the simulations for the cubic network film at equilibrium without cosolutes. The rectangular frames depict the actual simulation box of lengths L_x, L_y and L_z , shown for the following cases: (a) Stiff network with the rigidity constant $k_b = 10 k_B T$ and the intra-network interaction parameter $\epsilon_{nn} = 0.1 k_B T$ (i.e., corresponding to a good solvent). (b) Semi-flexible network with $k_b = 3 k_B T$ and $\epsilon_{nn} = 0.9 k_B T$, where the system is close to the network collapse transition point. (c) Collapsed semi-flexible network with $k_b = 3 k_B T$ and $\epsilon_{nn} = 2 k_B T$ (i.e., corresponding to a bad solvent).

work. The second one could be a higher-molecular weight polymer such as poly(N-isopropylacrylamide) (PNIPAM) or poly(methylmethacrylate) with more steric restraints and therefore stiffer conformations, leading to l_p values in the nanometer range [69–72]. Given our intra-bond Hamiltonian eq (2), the bending energy of our model polymers can be expressed by the persistence length l_p in the limit of small bending via [73–75]

$$l_p = \frac{2k_b\sigma}{k_B T}. \quad (4)$$

The bending rigidity of $k_b = 3 k_B T$, for example, yields the persistence length $l_p \approx 2$ nm, right in the reported range for PNIPAM. Hence, in the bulk part of our analysis we focus on two cases we define as flexible and semi-flexible networks with chosen rigidity constants $k_b = 0$ and $k_b = 3 k_B T$, respectively.

D. Two-component (network–cosolute) mean-field theory

With the purpose of establishing a firm theoretical model that mimics the simulation conditions and is able to explain the cosolute effects on the polymer network states, we develop a mean-field theory for a closed (canonical) system that contains the polymer gel (formed by interconnected and cross-linked monomeric units and

cosolutes) and the bulk reservoir (with only cosolutes). Therefore, the total number of cosolutes $N_c = N_c^{\text{in}} + N_c^{\text{out}}$ and the number of monomers in the gel phase N_n are both fixed quantities. The total Helmholtz free energy of such system can be written as $F = F_{\text{network}} + F_{\text{bulk}}$. The model essentially combines standard ideas from elastic polymer and network models[76], extended to include semi-flexibility via the worm-like chain approach [77, 78] and multi-component interactions on the virial expansion level [30]. Within these approximations, the free energy of the two-component network plus cosolute system is split into five different contributions:

$$F_{\text{network}} = F_{\text{ela}} + F_{\text{conf}} + F_{\text{ideal}} + F_{\text{HS}} + F_{\text{int}}. \quad (5)$$

The first contribution, F_{ela} , corresponds to the elastic free energy of the network. For semi-flexible and inextensible polymer chains, it can be approximated using the wormlike chain model as [77, 78]

$$\beta F_{\text{ela}} = N_{\text{ch}} \left[\frac{\pi^2 l_p}{2l} \{1 - (R/l)^2\} + \frac{2l}{\pi l_p} \frac{1}{1 - (R/l)^2} \right] \quad (6)$$

where R is the average end-to-end distance of the polymer chains between two cross-linkers, $l = N_m \sigma$ is the contour length (N_m is the number of monomers per chain), and N_{ch} is the number of chains of the network. In the limit of full stretching ($R \rightarrow l$) the elastic free energy diverges, as expected for inextensible chains. In the limit of small persistence length and weak stretch ($R \ll l$), this model tends to $\beta F_{\text{ela}} \approx \text{const.} + \frac{2R^2}{\pi N_m \sigma l_p}$, and for $l_p = 4\sigma/(3\pi)$ the Gaussian flexible chain is recovered. The second contribution in eq (5), F_{conf} , represents the (entropic) free energy of confinement that arises for highly collapsed states ($R \rightarrow 0$). It can be written as [79]

$$\beta F_{\text{conf}} = C N_{\text{ch}} \frac{\pi^2 N_m \sigma^2}{2 R^2}, \quad (7)$$

where C is a phenomenological normalization constant that depends on the network stiffness. This constant takes into account the fact that collapsing a stiff chain always implies a larger free energy than shrinking a flexible (Gaussian) chain. The third contribution is the ideal free energy of the cosolutes,

$$\beta F_{\text{ideal}} = c_c^{\text{in}} [\ln(c_c^{\text{in}} \Lambda_c^3) - 1] V_n, \quad (8)$$

where Λ_c is the thermal wavelength of the cosolute particles, V_n is the volume of the network, and $c_c^{\text{in}} = N_c^{\text{in}}/V_n$ is the number density of cosolutes inside the network. The fourth contribution is the hard sphere contribution, which takes into account the excluded-volume of the particles and prevents the interpenetration of monomers and cosolutes in conditions of strong inter-particle attractions. Assuming, just as in the simulations, that monomers and cosolutes have the same size, σ , this free energy is given by the Carnahan-Starling expression

$$\beta F_{\text{HS}} = \frac{4(\phi_n + \phi_c^{\text{in}}) - 3(\phi_n + \phi_c^{\text{in}})^2}{(1 - \phi_n - \phi_c^{\text{in}})^2} (c_n + c_c^{\text{in}}) V_n \quad (9)$$

where $c_n = N_n/V_n$ is the number density of monomers inside the network, $\phi_n = \pi c_n \sigma^3/6$ its packing fraction, and $\phi_c^{\text{in}} = \pi c_c^{\text{in}} \sigma^3/6$ is the packing fraction of cosolutes inside the network.

Finally, F_{int} is the interaction free energy between monomers and cosolute particles. Up to second order in the virial expansion of the monomer and cosolute number densities (c_n and $c_c \equiv c_c^{\text{in}}$, respectively), it is given by

$$\beta F_{\text{int}} = V_n \sum_{i,j=n,c} c_i c_j (B_2^{ij} - B_{2,\text{HS}}^{ij}) \quad (10)$$

where B_2^{ij} is the second virial coefficient for LJ interactions. In the expression we subtract the second virial coefficient for hard spheres ($B_{2,\text{HS}}^{ij} = 2\pi\sigma^3/3$), since this contribution has been already included in F_{HS} . The second virial coefficients can be calculated numerically for the different combinations of interparticle interaction strengths ϵ_{nn} , ϵ_{nc} , for a fixed intercosolute interaction $\epsilon_{cc} = 0.1 k_B T$.

To obtain the free energy of the bulk phase, F_{bulk} , we proceed in the same way and assume the same approximations, but with cosolutes as the only component

$$\beta F_{\text{bulk}} = \left[c_c^{\text{out}} (\ln(c_c^{\text{out}} \Lambda_c^3) - 1) + \frac{4\phi_c^{\text{out}} - 3(\phi_c^{\text{out}})^2}{(1 - \phi_c^{\text{out}})^2} c_c^{\text{out}} + (c_c^{\text{out}})^2 (B_2^{cc} - B_{2,\text{HS}}^{cc}) \right] V_{\text{bulk}} \quad (11)$$

where V_{bulk} is the volume of the bulk phase. Note that in this case we use the concentration of cosolutes in the bulk reservoir in the free energy expression, $c_c^{\text{out}} = N_c^{\text{out}}/V_{\text{bulk}}$, where $N_c^{\text{out}} = N_c - N_c^{\text{in}}$ to impose a constant total number of cosolutes in the whole system.

In order to compare with the simulation results, we assume that the contour length of the chains is $l = N_m \sigma = 5\sigma$, and that the polymer network has a cubic structure. The network is composed by 125 cubic cells, each one with a volume R^3 . Since each cell has 3 chains (with 4 interconnected monomer beads each) and 1 cross-linker monomer, the total volume of the network may be expressed as $V_n = N_{\text{ch}} R^3/3$, and the number density of network particles is $c_n = 13/R^3$. Following the morphology of the simulation box, we approximate in our theory $V_{\text{bulk}} \approx 2V_n$ for simplicity. Moreover, the total number of cosolute particles has been fixed in the theory to be $N_t = 576$. Therefore, the resulting total free energy of the system is, for a given temperature, a function of two variables, $F(N_c^{\text{in}}, V_n)$. In order to calculate the equilibrium swelling state of the gel network and the concentration of cosolutes absorbed inside we need to minimize the free energy against N_c^{in} and V_n at a constant pressure given by $p = 6.5853 \times 10^{-4} k_B T/\sigma^3$. This leads to the following non-linear set of algebraic equations:

$$\left(\frac{\partial F}{\partial N_c^{\text{in}}} \right) = 0 \quad \text{and} \quad \left(\frac{\partial F}{\partial V_n} \right) = -3p \quad (12)$$

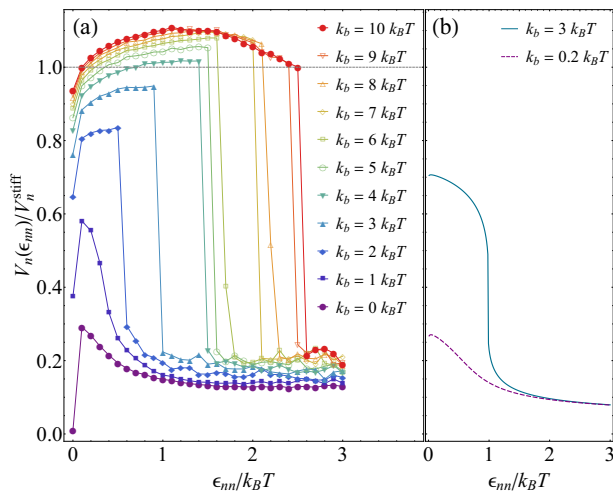


FIG. 2. Mean network volumes $V_n(\epsilon_{nn})/V_n^{\text{stiff}}$ depending on solvent quality parameter ϵ_{nn} for various network bending rigidities k_b . (a) Simulation results. (b) Theoretical predictions for semi-flexible ($k_b/k_B T = 3$) network and flexible ($k_b/k_B T = 0.2$) network, based on the mean-field theory in Section IID.

where the factor of 3 in the last equation comes from the fact that the entire volume of the system is $3V_n$.

We use this model to determine the swelling behavior of the network for two different conditions of chain bending rigidities, namely flexible ($l_p = 4\sigma/(3\pi)$, $k_b \approx 0.2 k_B T$) and semi-flexible ($l_p = 6\sigma$, $k_b = 3 k_B T$). The phenomenological constant C in eq (7) for the flexible chains is $C = 1$, and the resulting swelling curve predicted by the mean-field theory is in very good agreement with the simulation result (for example, see Figure. 2) with no free fitting parameters. For semi-flexible chains, we use a fitted value of $C = 3$ at which yields the collapse transition around $\epsilon_{nn} = 1 k_B T$ as shown in Figure. 2(b), resulting in qualitative agreement of the theory with the simulation results.

III. RESULTS AND DISCUSSION

A. Cosolute-free networks

1. Volume transition

Before we present results on cosolute partitioning we briefly discuss the network properties for the cosolute-free reference systems. Figure 2 shows the mean network volume $V_n(\epsilon_{nn}) \equiv \langle A(\epsilon_{nn})d(\epsilon_{nn}) \rangle$, where $A(\epsilon_{nn})$ is the area in the xy plane and $d(\epsilon_{nn})$ is the thickness of the film, respectively. The mean volume is rescaled by V_n^{stiff} , the mean volume of a stiff and repulsive reference network with $k_b = 10 k_B T$ and $\epsilon_{nn} = 0.1 k_B T$. The mean volume exhibits dramatic changes with varying k_b and ϵ_{nn} . For $\epsilon_{nn} = 0$, the equilibrium volumes increase with k_b , which can be readily understood by the larger stiffness

of the network chains. As ϵ_{nn} increases from zero (i.e., from perfectly ideal polymer to a good solvent state), V_n substantially increases overall due to the excluded repulsion between the neighboring network beads. The larger the network bending rigidities the smaller the effect. As the effective interaction parameter ϵ_{nn} further increases (moving towards a bad solvent), there are two opposing effects that result in two different trends depending on the chain rigidity: First, the attraction depth of the LJ interaction increases, but secondly also the excluded volume repulsion slightly increases with growing ϵ_{nn} (since it is also a prefactor of the repulsive LJ term). For the less flexible chains ($k_b \gtrsim 2 k_B T$), only little inter-bead interactions are present, mostly only bonded, nearest-neighbor interactions. In this case, the excluded-volume effect dominates in our model and the network swells slightly. For the more flexible systems ($k_b \lesssim 2 k_B T$) there are more many-bead interactions and the overall increased attraction outweighs the steric exclusion, as expected for a simple LJ fluid.

More importantly, further increase of ϵ_{nn} leads to a discontinuous collapse transition for semi-flexible and stiff chains ($k_b \gtrsim 2 k_B T$). This abrupt drop-down of the polymer volume [39, 48] is correlated to the breakdown of the network structure. The critical attraction for the collapse increases from $\epsilon_{nn} \approx 0.6$ to $2.6 k_B T$ for the stiffest chains. For very large ϵ_{nn} , all networks saturate almost to the same (closed-packed) limit around $V_n/V_n^{\text{stiff}} = 0.2$. For the semi-flexible network film, where the collapse transition occurs around the transition point $\epsilon_{nn} = 1 k_B T$ (Figure 2), the volume fluctuations are extremal around the transition point (see Figure S7 in SI), as qualitatively expected from experimental knowledge [26, 39]. The transition is continuous for the more flexible chains, as known from previous theories for polymer collapse transitions, either on a single chain level [80] or the network level using the Flory rubber elasticity [20–22] and combination of the bending energy and Flory–Huggins theory in the rod limit [23]. The transition behavior observed in the simulations can also be semi-quantitatively reproduced by the mean-field theory (without cosolutes), as shown in Figure 2(b). In particular, the theory clearly shows the effect of the gel semi-flexibility on the sharp volume transition, i.e., as in the simulations the transition is continuous for the flexible chains, and becomes discontinuous for semi-flexible chains. This is in fact also consistent with experiments of PNIPAM networks whose volume transitions are discontinuous above a certain cross-linking degree which can not be described by simple Gaussian mean-field theories (like Flory–Huggins) and was ascribed to both flexibility and defect effects [81]. Our results suggest that solely a diminished flexibility is already sufficient to push a strongly cross-linked system to discontinuous volume transitions.

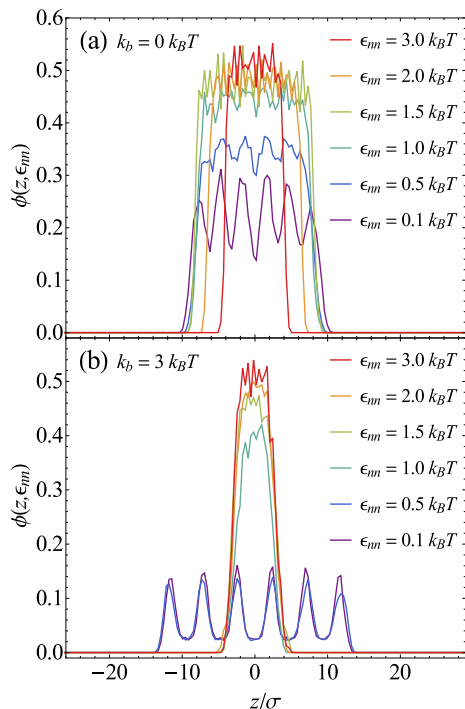


FIG. 3. Mean network monomer density profiles (packing fraction) $\phi(z, \epsilon_{nn})$ for (a) flexible ($k_b/k_B T = 0$) and (b) semi-flexible ($k_b/k_B T = 3$) polymers at various values of ϵ_{nn} , see the legend.

2. Monomer packing fraction profiles

The collapse transition of the network is also clearly visible in the local packing fraction resolved in z , $\phi(z, \epsilon_{nn}) = v c_n(z, \epsilon_{nn})$, where $v = \pi\sigma^3/6$ represents the volume of a single bead, and $c_n(z, \epsilon_{nn})$ is the local number density. In Figure 3, $\phi(z)$ for the semi-flexible and flexible network films is shown for various values of the solvent quality parameter ϵ_{nn} , respectively. The packing fraction is overall transformed from a structured shape with salient multiple peaks into a predominant single broad peak, signifying the collapsed state after ϵ_{nn} crosses the volume transition value. However, as discussed above, the flexible network (Figure 3(a)) collapses rather continuously and maintains a characteristically ordered structure even up to $\epsilon_{nn} = 1 k_B T$, whereas the semi-flexible network structure collapses abruptly (Figure 3(b)), and a peak fluctuates around the center $z = 0$. Note that the integral over the profiles yields the monomer number density per area and is not a conserved quantity as the aspect ratio of the network (i.e., the ratio of the length in x or y to the width in z) depends on the flexibility and ϵ_{nn} .

B. Networks including cosolutes

We now consider effects of interacting cosolute particles. Hence, in addition to the intrinsic solvent quality parameter ϵ_{nn} , we now study the influence of varying the network–cosolute interactions given by ϵ_{nc} , i.e., the cosolute coupling parameter.

1. Network-cosolute state diagram

Figure 4 shows in the central panel (colored landscape) the mean film width d/σ of the semi-flexible network in dependence of both interaction parameters along with representative simulation snapshots. We now study the width instead of the total volume to distinguish better the effects on the aspect ratio of the network. We see that there are overall five regions and a critical line that characterizes the collapse transition. We classify these regions into “swollen”, “collapsed”, “cosolute-induced collapsed”, “cosolute-adsorbed collapsed”, and “cosolute-involved collapsed” states, as depicted on the landscape. Hence, in addition to the intrinsic volume transition between the “swollen” (c) and the “collapsed” (f) states, on which the rapid color change from the red (swollen) region to the blue (collapsed) region is notable as yellow ‘critical’ line (b), we observe three new cosolute-related states.

Most importantly, we find cosolute-induced collapsed states (a), in which even in a good solvent condition, the network can undergo a sharp collapse transition triggered by the strong cosolute attraction to the monomers. The reason for this cosolute-induced collapse is a high energy gain of the system by bridging cosolutes located between multiple attracted monomers. The existence of those has been demonstrated before only for single chains by computer simulations and statistical theory [30, 82–85] as well as experiments. [86–88] Evidently, this effect also plays a role in polymer networks.

In the “cosolute-involved” collapsed state (d), where the solvent quality ranges from $\epsilon_{nn} \approx 0.2 k_B T$ to $\epsilon_{nn} \approx 1.6 k_B T$ and the cosolute coupling is strong, $\epsilon_{nc} > 1.8 k_B T$, the network is intrinsically in the collapsed regime but also embeds the attracted cosolutes. In this state, the gel volume becomes approximately two times larger than the collapsed volume in a bad solvent without cosolutes embedded. Finally, in the “cosolute-adsorbed collapsed” state (e), where both network–network and network–cosolute attractions are strong, the network is collapsed and cosolutes are attracted to the surface of the network but do not penetrate it. However, these two states “cosolute-involved collapsed” and “cosolute-adsorbed collapsed” are not clearly distinguishable as it is not well defined in which parameter region they are actually equilibrium states. Their exact stability regions may depend on the simulation history and could originate from kinetically trapped trajectories due to the strong attractions involved.

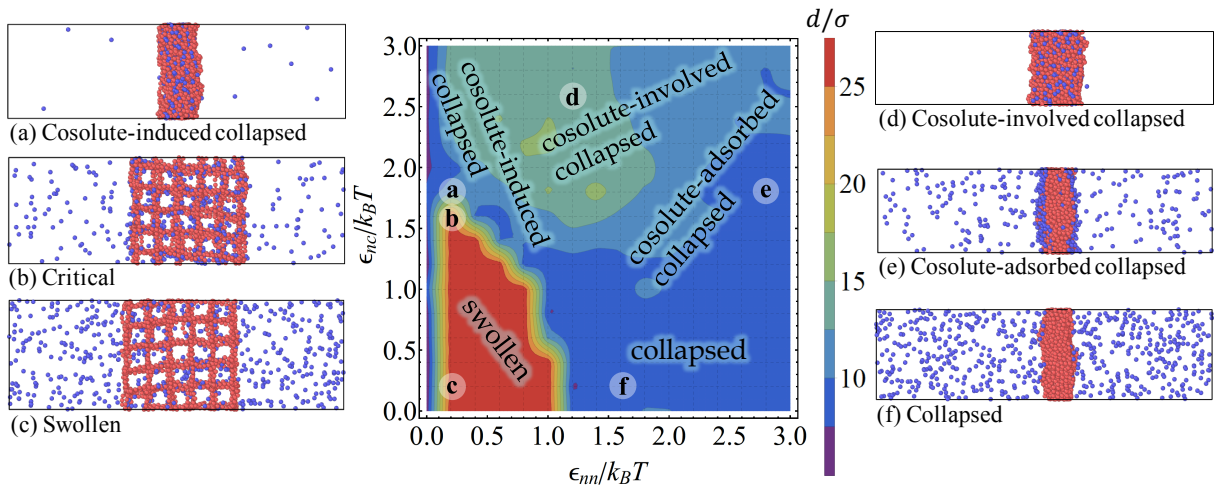


FIG. 4. Center: The mean width d of the semi-flexible network film, as a function of both the solvent quality parameter ϵ_{nn} and the cosolute coupling parameter ϵ_{nc} . The regions on the landscape are classified into “swollen”, “collapsed”, “cosolute-induced collapsed”, “cosolute-involved collapsed”, and “cosolute-adsorbed collapsed” states illustrated by representative simulation snapshots: (a) The cosolute-induced collapsed state in a good solvent ($\epsilon_{nn} = 0.2 k_B T$) and strong cosolute coupling ($\epsilon_{nc} = 1.8 k_B T$) conditions. The collapse transition is induced by high attraction between the network and the cosolute particles although the network intrinsically favors the swollen structure. (b) The critical swollen state in a good solvent ($\epsilon_{nn} = 0.2 k_B T$) and less strong cosolute coupling ($\epsilon_{nc} = 1.6 k_B T$) conditions. (c) The swollen state in a good solvent ($\epsilon_{nn} = 0.2 k_B T$) and weak cosolute coupling ($\epsilon_{nc} = 0.2 k_B T$). (d) The cosolute-involved collapsed state in a bad solvent ($\epsilon_{nn} = 1.2 k_B T$) and very strong cosolute coupling ($\epsilon_{nc} = 2.6 k_B T$) conditions. Due to the large attraction between the cosolutes and the network, the film width is larger than the other collapsed states. (e) The cosolute-adsorbed collapsed state in a very bad solvent ($\epsilon_{nn} = 2.8 k_B T$) and strong cosolute coupling ($\epsilon_{nc} = 1.8 k_B T$) conditions. The collapse transition is induced by high attraction between network particles, yielding the cosolute particle adsorption onto the network surfaces. (f) The collapsed structure in a bad solvent ($\epsilon_{nn} = 1.6 k_B T$) and weak cosolute coupling ($\epsilon_{nc} = 0.2 k_B T$).

2. Impact of cosolutes on the volume transition

In Figure 5 we plot the mean network volume $V_n(\epsilon_{nn}, \epsilon_{nc})$ in a more quantitative representation for both flexible and semi-flexible models versus ϵ_{nn} (for various ϵ_{nc}) or versus ϵ_{nc} (for various ϵ_{nn}). For the flexible network, disregarding the jump when going from a non-interacting to interacting polymer at small $\epsilon_{nn} \simeq 0.1 k_B T$, the volume decreases continuously without any sharp transition irrespective of the cosolute interaction, see panel (a). For fixed solvent quality, only in very good solvents, $\epsilon_{nn} \simeq 0.2 k_B T$, the change with cosolute interaction is substantial, see panel (b), where large network-cosolute attractions strongly collapse the network. For poorer solvents the network is always collapsed without much change induced by the cosolutes. For the semi-flexible network film, panels (e) and (f), the sharp volume transitions are recovered. The transition shifts to smaller network attractions ϵ_{nn} for larger cosolute attraction, see panel (e). This is a signature of the cosolute-induced collapse we discussed above. The same signature can be found for good solvents in panel (f). We note that we also observe that the volume fluctuations of semi-flexible network films are maximized around the respective transition lines and that cosolute fluctuations inside the network are intimately coupled to them, see SI.

The features and trends reported in the simulations are also captured by the mean-field theory presented in eqs (5)–(11). Figures 5(c) and (d) show, respectively, the network volume predicted by this theory as a function of ϵ_{nn} and ϵ_{nc} for flexible chains. We observe that, including non-interacting cosolutes in the system ($\epsilon_{nc} = 0$) leads to the swelling of the network due to the ideal gas contribution to the pressure induced by the density of the non-interacting cosolutes, which has to be compensated by the expanded network to keep the overall pressure constant. This swelling is emphasized when we increase the cosolute-monomer repulsion ($\epsilon_{nc} \approx 0.2 k_B T$). A similar finding has been reported for the swelling of charged microgels in salty media when the excluded-volume repulsive interactions exerted by the polymer network are taken into consideration. [89] However, as soon as we increase ϵ_{nc} beyond $0.6 k_B T$, the monomer-cosolute attraction leads to a progressive shrinking of the network for small values of ϵ_{nn} . This is a clear evidence of the cosolute-induced collapse, by which a network in good solvent conditions (swollen) tends to collapse in the presence of very attractive cosolutes.

On the other hand, if we consider an already collapsed network in a bad solvent (moderate and large values of ϵ_{nn}), for relatively small values of ϵ_{nc} the cosolutes tend to be excluded from the network, and so they are expected to surface-adsorb (although the theoretical model is not able to study the adsorption, it does predict the exclusion from the network). However, further enhancement of network-cosolute attraction leads finally to an increase of the network volume. In this case, the collapsed network is forced to swell to permit the strongly

attractive cosolutes to diffuse inside.

Figure 5(d) provides a very instructive illustration of the role of the cosolute network interaction. Increasing ϵ_{nc} leads first to an increase of the network volume. Indeed, for moderate attractions, the network swells to increase the contact surface exposed by the polymer chains allowing the attractive cosolutes to diffuse inside. However, if we increase more ϵ_{nc} , the multiple contacts between monomers and cosolutes finally induce the network collapse with the cosolutes embedded inside; the so-called cosolute-involved collapse. This leads to the appearance of a maximum that, although is only weakly established in the simulations, it is in fact a known effect [30].

Figures 5(g) and (h) depict again the swelling response of the polymer network but for semi-flexible chains. As observed, the simulation and theory swelling and transition trends with cosolutes are fully consistent. Indeed, the theory predicts a shift of the sharp volume transition to larger values of ϵ_{nn} for effective cosolute-monomer repulsions. Then, by increasing ϵ_{nc} above $0.3 k_B T$, the transition moves to smaller values of ϵ_{nn} , indicating that the attractive cosolute is causing the cosolute-induced collapse. For $\epsilon_{nc} \gtrsim 1.5 k_B T$ the attraction is so strong that it is able to fully collapse the network even for good solvent conditions. Moreover, for moderate to large values of ϵ_{nn} the theory also predicts the cosolute-involved collapse reported in the simulations for intense cosolute-monomer attractions.

3. Cosolute packing fraction profiles

The mean local packing fractions $\phi_n(z)$ of the network particles and $\phi_c(z)$ of the cosolutes are shown in Figure 6, for the semi-flexible (red) and flexible (blue) network films. In this matrix representation, the network solvent quality decreases from top to bottom and the cosolute coupling increases from left to right. Hence, at the bottom we see signatures of more collapsed states, and moving to the right we see more cosolutes at or inside the network. Some details, however, are rather complex. For instance, a cosolute-induced collapse transition is found in (b)→(c) for the semi-flexible films, in contrast to the cosolute-induced transition for the flexible films: The transition (d)→(f) is rather a swelling transition where the cosolutes inside the flexible network strengthen the network structure. The latter effect is due to a collective adsorption of the cosolutes accumulating particularly at the network cross-linkers [90], which in conjugation with the gel flexibility maintains the network structure. In the weak cosolute coupling regime, as shown in Figures 6(a), (d) and (g), the cosolutes favor predominantly being outside the network film, throughout the entire collapse transition due to the change of the solvent quality. A combination of the bad solvent quality and the strong cosolute coupling, as shown in Figures 6(e), (f), (h) and (i), enhances the cosolutes cumulation not only into the network film but also on the

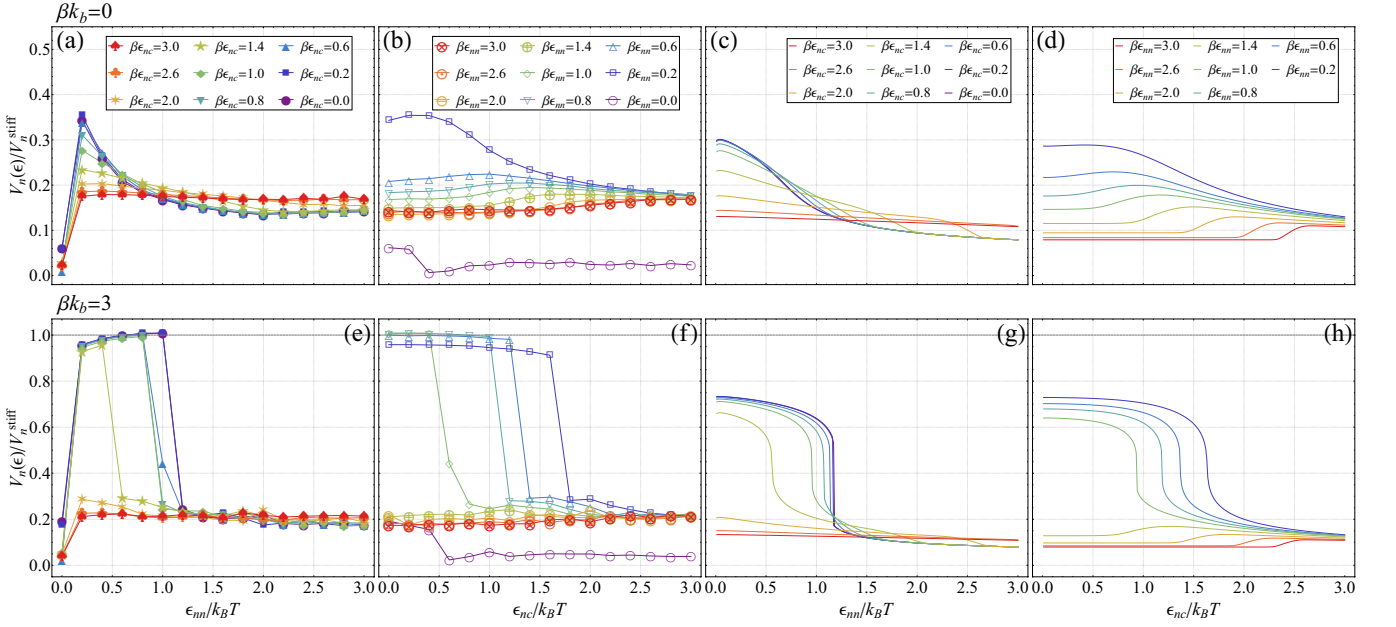


FIG. 5. Simulation results for mean network film volumes $V_n(\epsilon)/V_n^{\text{stiff}}$ depending on (a) $\epsilon_{nn}/k_B T$, (b) $\epsilon_{nc}/k_B T$ for the flexible network film, (e) $\epsilon_{nn}/k_B T$, and (f) $\epsilon_{nc}/k_B T$ for the semi-flexible network film. Theoretical predictions as functions of (c) $\epsilon_{nn}/k_B T$, (d) $\epsilon_{nc}/k_B T$ for the flexible network film, (g) $\epsilon_{nn}/k_B T$, and (h) $\epsilon_{nc}/k_B T$ for the semi-flexible network film. The mean-field theory (eqs (5)–(12)), as a function of the solvent quality parameter ϵ_{nn} for flexible networks ($l_p = 0.43\sigma$, upper panels) and semi-flexible networks ($l_p = 6\sigma$, bottom panels) is used.

interface between the film and the bulk, leading to a high surface adsorption effect.

4. Cosolute global partitioning

We finally investigate the cosolutes' global partitioning. It is computed using the definition $\mathcal{K}(\epsilon_{nn}, \epsilon_{nc}) = \phi_c^{\text{in}}/\phi_c^{\text{out}}$ where the mean cosolute packing fraction inside the film is computed as $\phi_c^{\text{in}} = \int_{\text{in}} dz \phi_c(z)/\Delta l_{\text{in}}$ integrating over the width Δl_{in} of the film, and the mean cosolute packing fraction outside the network is computed as $\phi_c^{\text{out}} = \int_{\text{out}} dz \phi_c(z)/(Lz - \Delta l_{\text{in}} - 2l_{\text{surf}})$ over the range outside the network. Here we subtract the surface effects on the cosolutes by carefully choosing the surface width l_{surf} around the film–bulk interfaces, respectively depending on ϵ_{nn} and ϵ_{nc} (see Figures S4 and S5 in SI). We note that we also computed the fluctuations of the local packing fractions $\Delta\phi_{n,c}^2(z)$, i.e., the variance of $\phi_{n,c}(z)$, to obtain partitioning fluctuations. (see Figure S6 in SI).

The partitioning \mathcal{K} is related to the transfer free energy $\Delta G = -k_B T \ln \mathcal{K}$, a measure of the effective cosolute–network interaction. We show $\Delta G(\epsilon_{nn}, \epsilon_{nc})$ in Figures 7(a) and (c). The partitioning depends not only on the cosolute coupling but also significantly on the solvent quality. The cosolute uptake is largely affected by the solvent quality, particularly when the film collapses in a bad solvent and with weak cosolute couplings. For the two different network film models, ΔG shows different shapes of the landscapes, reflecting significant role of the net-

work flexibility. The transfer energy overall becomes attractive as the cosolute coupling increases, however, ΔG for the semi-flexible film has a large zero-energy region, particularly in the swollen zone (see Figure 4), which is not seen in ΔG for the flexible films. The slow relaxation of the trapped cosolutes in the flexible network films at $\epsilon_{nn} > 1.4 k_B T$ in the weak cosolute coupling results in a strong cosolute trapping effect on ΔG with maximal repulsion. In this case, the flexible network collapses exceedingly faster than the cosolutes relaxation, thus the cosolutes are trapped in the collapsed network for a long time (beyond our total simulation time) before they are equilibrated by diffusing out of the network, i.e., crossing over the large barrier to an energy minimum. We depict this metastable parameter zone which gives rise to the strong cosolute trapping effect by a dashed line in Figure 7(a). Note that the gel collapse transition can occur at both extrema of ΔG .

Figures 7(b) and (d) show the transfer free energy ΔG depending on the cosolute coupling ϵ_{nc} for different values of the solvent quality parameter ϵ_{nn} , depicted by dotted lines in panels (a) and (c). As the cosolute coupling increases, ΔG decreases, particularly signalling the cosolute-induced collapse in a good solvent condition. For the semi-flexible film this reduction of ΔG shown in Figure 7(d) is dramatic, that is, abruptly decreasing around the collapse transition point in a good solvent condition.

The simple mean-field partitioning theory presented in Section IID can also be applied to determine the ra-

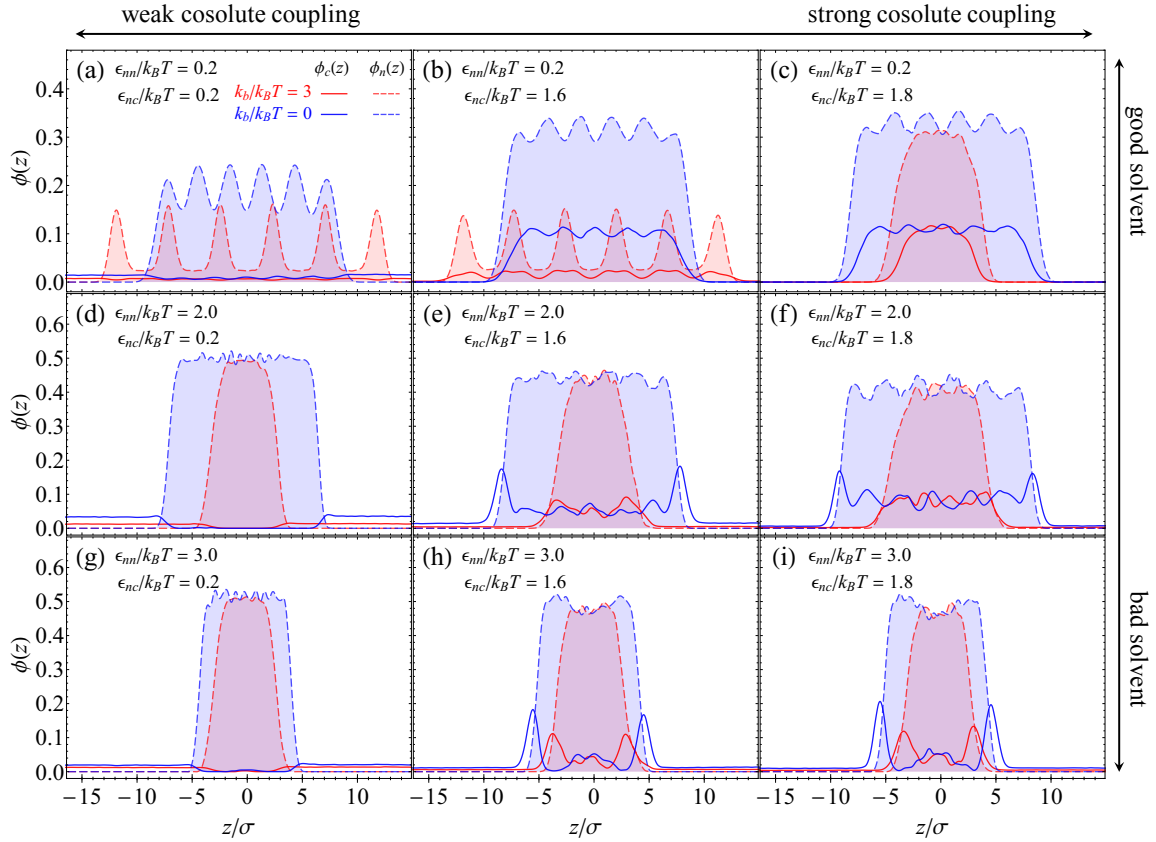


FIG. 6. Mean local packing fractions $\phi_n(z)$ of network particles (dashed lines) and $\phi_c(z)$ of cosolute particles (solid lines), for semi-flexible (red) and flexible (blue) network films, at various values of the interaction parameters ϵ_{nn} and ϵ_{nc} .

tio of concentrations of cosolutes inside and outside the network and, from them, the desired transfer free energy $\beta\Delta G = -\ln(c_c^{\text{in}}/c_c^{\text{out}})$. The results for $\Delta G(\epsilon_{nc})$ are shown by solid lines in Figures 7(b) and (d) for flexible and semi-flexible networks, respectively. Good agreement of the theoretical prediction with the simulation results is found. In general, the theoretical results confirm that increasing the network–cosolute attraction leads to an increase of the cosolute concentration, which corresponds to more negative adsorption energies for both, flexible and stiff networks. For the case of a polymer network in a bad solvent, the gel phase is already collapsed. In this particular situation, cosolutes are strongly excluded from the gel phase as they disrupt the attractive bonds between neighboring monomers. As a result of this, very large and positive transfer free energies are predicted in this regime, and only for relative large cosolute–network attractions (about $\epsilon_{nc} \gtrsim 1 k_B T$) the transfer free energy becomes negative. This effect is also well captured by the mean-field theory, in accordance with the simulation data (see solid lines in Figures 7(b) and (d)). Moreover, in some cases the theory shows to be remarkably good, as it even provides quantitative agreement with the simulation results, especially for moderate inter-monomer attractions (see for instance that the model is able to capture the abrupt decrease of the free

energy induced by the cosolute attraction, achieved for semi-flexible networks in good solvent conditions).

IV. SUMMARY AND CONCLUDING REMARKS

In summary, we studied the partitioning of model cosolutes to a simple cubic polymer network film for a wide range of solvent qualities and interactions by using extensive coarse-grained computer simulations, with special focus on the influence of polymer flexibility and volume transitions. In addition, the computer simulation results were corroborated by the theoretical predictions for the network swelling and the cosolute partitioning obtained with a two-component mean-field approach that takes into account the chain flexibility, the excluded-volume effects and the role of the attractive interaction up to second order in the virial expansion. A sharp discontinuous collapse transition was found only in semi-flexible networks, in agreement with a newly developed mean-field theory. Our simulations and theory are generic in a sense that the interaction parameters ϵ_{nn} and ϵ_{nc} consider multiple combinations of effective interactions, going from repulsive to attractive pair interactions.

In the presence of cosolutes we then found a rich

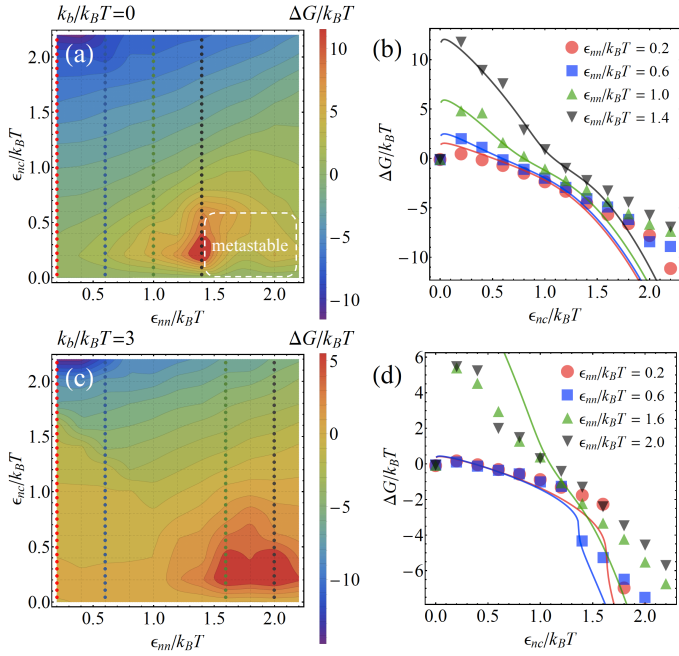


FIG. 7. For flexible network films: (a) Adsorption energy profile $\Delta G(\epsilon_{nn}, \epsilon_{nc})$, (b) $\Delta G(\epsilon_{nc})$ (symbols) for different values of $\epsilon_{nn} = 0.2, 0.6, 1.0$, and $1.4 k_B T$. The solid lines depict the theory prediction for ΔG . For semi-flexible network films: (c) Adsorption energy profile $\Delta G(\epsilon_{nn}, \epsilon_{nc})$, (d) $\Delta G(\epsilon_{nc})$ (symbols) for different values of $\epsilon_{nn} = 0.2, 0.6, 1.6$, and $2 k_B T$. The solid lines depict the theory prediction for ΔG . The dotted lines in (a) and (c) denote respective fixed values of ϵ_{nn} used in (b) and (d).

and nontrivial topology of equilibrium gel structural states and partitioning despite the simplicity of the models. In particular, the network film width revealed that there are overall five distinct states that characterize a measure of the collapse transition, and we categorized these states into “swollen”, “collapsed”, and “cosolute-induced”, “cosolute-involved”, “cosolute-adsorbed” collapsed states. The “cosolute-induced” collapsed state is noteworthy, showing a collective manner of the network collapse transition which is induced by the cosolutes in the strong cosolute coupling, even in good solvents,

and accompanied by maximal but finite collective fluctuations. In addition, the “cosolute-involved” collapsed state occurs in intermediate solvent conditions, and the “cosolute-adsorbed” collapsed state occurs in bad solvent conditions.

The global adsorption energy landscape computed via the cosolutes partitioning exhibits very different topologies on two different gel models, particularly showing the distinct swollen states in the semi-flexible gels. For the flexible gel system the collapse transition driven by bad solvents and weak cosolute couplings results in a very strong trapping of the cosolutes inside the gel, giving rise to metastable states. Finally, we compared the volume transition and transfer free energy with a theoretical model. By using the mean-field level virial expansion, we found a good qualitative agreement of the theory with the simulation results.

The coarse-grained model based on the simple cubic network [44, 45, 61–64] entails further extension towards more realistic gel structures, e.g., multi-functional gels with random cross-linkings and defects. Quantifying the partitioning and fluctuations in those systems depending on structural properties such as polydispersity [50], as well as their coupling to cosolute diffusion and permeability[16], would be a fecund future work. With these extensions of simulations as well as predictive theory the future rational design and development of soft functional materials will be hopefully facilitated.

ACKNOWLEDGMENTS

The authors thank Matthias Ballauff and Richard Chudoba for fruitful discussions. This project has received funding from the European Research Council (ERC) under the European Union’s Horizon 2020 research and innovation programme (grant agreement No. 646659-NANOREACTOR). A.M.-J. acknowledge funding by the Spanish ‘Ministerio de Economía y Competitividad (MINECO), Plan Nacional de Investigación, Desarrollo e Innovación Tecnológica (I+D+i)’ (Project FIS2016-80087-C2-1-P). The simulations were performed with resources provided by the North-German Supercomputing Alliance (HLRN).

[1] Peppas, N.; Bures, P.; Leobandung, W.; Ichikawa, H. Hydrogels in pharmaceutical formulations. *Eur. J. Pharm. Biopharm.* **2000**, *50*, 27–46.
 [2] Hamidi, M.; Azadi, A.; Rafei, P. Hydrogel nanoparticles in drug delivery. *Adv. Drug Delivery Rev.* **2008**, *60*, 1638–1649.
 [3] Tokarev, I.; Minko, S. Stimuli-Responsive Porous Hydrogels at Interfaces for Molecular Filtration, Separation, Controlled Release, and Gating in Capsules and Membranes. *Adv. Mater.* **2010**, *22*, 3446–3462.
 [4] Stuart, M. A. C.; Huck, W. T.; Genzer, J.; Müller, M.;

Ober, C.; Stamm, M.; Sukhorukov, G. B.; Szleifer, I.; Tsukruk, V. V.; Urban, M.; Winnik, F.; Zauscher, S.; Luzinov, I.; Minko, S. Emerging applications of stimuli-responsive polymer materials. *Nat. Mater.* **2010**, *9*, 101–113.
 [5] Lu, Y.; Ballauff, M. Thermosensitive core-shell microgels: from colloidal model systems to nanoreactors. *Prog. Polym. Sci.* **2011**, *36*, 767–792.
 [6] Welsch, N.; Ballauff, M.; Lu, Y. *Chemical design of responsive microgels*; Springer, 2010; pp 129–163.
 [7] Lu, Y.; Mei, Y.; Drechsler, M.; Ballauff, M. Thermosen-

- sitive core-shell particles as carriers for Ag nanoparticles: modulating the catalytic activity by a phase transition in networks. *Angew. Chem. Int. Ed.* **2006**, *45*, 813–816.
- [8] Ballauff, M.; Lu, Y. “Smart” nanoparticles: preparation, characterization and applications. *Polymer* **2007**, *48*, 1815–1823.
- [9] Menne, D.; Pitsch, F.; Wong, J. E.; Pich, A.; Wessling, M. Temperature-Modulated Water Filtration Using Microgel-Functionalized Hollow-Fiber Membranes. *Angew. Chem. Int. Ed.* **2014**, *53*, 5706–5710.
- [10] Plamper, F. A.; Richtering, W. Functional Microgels and Microgel Systems. *Acc. Chem. Res.* **2017**, *50*, 131–140.
- [11] Wu, C.; Yan, C.-Y. Studies of the swelling and drying kinetics of thin gelatin gel films by in situ interferometry. *Macromolecules* **1994**, *27*, 4516–4520.
- [12] Zhou, S.; Wu, C. In-situ interferometry studies of the drying and swelling kinetics of an ultrathin poly (N-isopropylacrylamide) gel film below and above its volume phase transition temperature. *Macromolecules* **1996**, *29*, 4998–5001.
- [13] Lobaskin, V.; Bogdanov, A. N.; Vinogradova, O. I. Interactions of neutral semipermeable shells in asymmetric electrolyte solutions. *Soft Matter* **2012**, *8*, 9428–9435.
- [14] Petrache, H. I.; Tristram-Nagle, S.; Harries, D.; Kučerka, N.; Nagle, J. F.; Parsegian, V. A. Swelling of phospholipids by monovalent salt. *J. Lipid Res.* **2006**, *47*, 302–309.
- [15] Leo, A.; Hansch, C.; Elkins, D. Partition coefficients and their uses. *Chem. Rev.* **1971**, *71*, 525–616.
- [16] Gehrke, S.; Fisher, J.; Palasis, M.; Lund, M. E. Factors determining hydrogel permeability. *Ann. N. Y. Acad. Sci.* **1997**, *831*, 179–207.
- [17] Angioletti-Uberti, S.; Lu, Y.; Ballauff, M.; Dzubiella, J. Theory of Solvation-Controlled Reactions in Stimuli-Responsive Nanoreactors. *J. Phys. Chem. C* **2015**, *119*, 15723–15730.
- [18] Roa, R.; Kim, W. K.; Kanduč, M.; Dzubiella, J.; Angioletti-Uberti, S. Catalyzed Bimolecular Reactions in Responsive Nanoreactors. *ACS Catal.* **2017**, DOI: 10.1021/acscatal.7b01701.
- [19] Shibayama, M.; Tanaka, T. *Responsive gels: Volume transitions I*; Springer, 1993; pp 1–62.
- [20] Khokhlov, A. Swelling and collapse of polymer networks. *Polymer* **1980**, *21*, 376–380.
- [21] Erman, B.; Flory, P. Critical phenomena and transitions in swollen polymer networks and in linear macromolecules. *Macromolecules* **1986**, *19*, 2342–2353.
- [22] Khokhlov, A.; Starodubtzev, S.; Vasilevskaya, V. *Responsive gels: Volume transitions I*; Springer, 1993; pp 123–171.
- [23] Barenbrug, T. M.; Smit, J.; Bedeaux, D. Highly swollen gels of semi-flexible polyelectrolyte chains near the rod limit. *Polymer Gels and Networks* **1995**, *3*, 331–373.
- [24] Heskins, M.; Guillet, J. E. Solution Properties of Poly(N-isopropylacrylamide). *J. Macromol. Sci., Chem.* **1968**, *2*, 1441–1455.
- [25] Dušek, K.; Patterson, D. Transition in swollen polymer networks induced by intramolecular condensation. *J. Polym. Sci. A-2 Polym. Phys* **1968**, *6*, 1209–1216.
- [26] Habicht, A.; Schmolke, W.; Goerigk, G.; Lange, F.; Saalwächter, K.; Ballauff, M.; Seiffert, S. Critical fluctuations and static inhomogeneities in polymer gel volume phase transitions. *J. Polym. Sci. B Polym. Phys.* **2015**, *53*, 1112–1122.
- [27] Wu, C.; Zhou, S. Volume phase transition of swollen gels: discontinuous or continuous? *Macromolecules* **1997**, *30*, 574–576.
- [28] Schild, H. G.; Muthukumar, M.; Tirrell, D. A. Cononsolvency in mixed aqueous solutions of poly(N-isopropylacrylamide). *Macromolecules* **1991**, *24*, 948–952.
- [29] Zhang, Y.; Cremer, P. Chemistry of Hofmeister Anions and Osmolytes. *Annu. Rev. Phys. Chem.* **2010**, *61*, 63–83.
- [30] Heyda, J.; Muzdalo, A.; Dzubiella, J. Rationalizing polymer swelling and collapse under attractive cosolvent conditions. *Macromolecules* **2013**, *46*, 1231–1238.
- [31] Heyda, J.; Dzubiella, J. Thermodynamic Description of Hofmeister Effects on the LCST of Thermosensitive Polymers. *J. Phys. Chem. B* **2014**, *118*, 10979–10988.
- [32] Zhao, Y.; Zhang, G.; Wu, C. Nonergodic dynamics of a novel thermally sensitive hybrid gel. *Macromolecules* **2001**, *34*, 7804–7808.
- [33] Moncho-Jordá, A.; Anta, J.; Callejas-Fernández, J. Effective electrostatic interactions arising in core-shell charged microgel suspensions with added salt. *J. Chem. Phys.* **2013**, *138*, 134902.
- [34] Moncho-Jordá, A. Effective charge of ionic microgel particles in the swollen and collapsed states: The role of the steric microgel-ion repulsion. *J. Chem. Phys.* **2013**, *139*, 064906.
- [35] Moncho-Jordá, A.; Adroher-Benítez, I. Ion permeation inside microgel particles induced by specific interactions: from charge inversion to overcharging. *Soft Matter* **2014**, *10*, 5810–5823.
- [36] Adroher-Benítez, I.; Moncho-Jordá, A.; Dzubiella, J. Sorption and Spatial Distribution of Protein Globules in Charged Hydrogel Particles. *Langmuir* **2017**, *33*, 4567–4577.
- [37] Kanduč, M.; Chudoba, R.; Palczynski, K.; Kim, W. K.; Roa, R.; Dzubiella, J. Selective solute adsorption and partitioning around single PNIPAM chains. *Phys. Chem. Chem. Phys.* **2017**, *19*, 5906–5916.
- [38] Tanaka, T. Collapse of gels and the critical endpoint. *Phys. Rev. Lett.* **1978**, *40*, 820–823.
- [39] Tanaka, T.; Ishiwata, S.; Ishimoto, C. Critical Behavior of Density Fluctuations in Gels. *Phys. Rev. Lett.* **1977**, *38*, 771–774.
- [40] Mann, B. A.; Everaers, R.; Holm, C.; Kremer, K. Scaling in polyelectrolyte networks. *Europhys. Lett.* **2004**, *67*, 786–792.
- [41] Duering, E. R.; Kremer, K.; Grest, G. S. Structure and relaxation of end-linked polymer networks. *J. Chem. Phys.* **1994**, *101*, 8169–8192.
- [42] Escobedo, F. A.; de Pablo, J. J. Simulation and theory of the swelling of athermal gels. *J. Chem. Phys.* **1997**, *106*, 793–810.
- [43] Escobedo, F. A.; De Pablo, J. J. Molecular simulation of polymeric networks and gels: phase behavior and swelling. *Phys. Rep.* **1999**, *318*, 85–112.
- [44] Aydt, E.; Hentschke, R. Swelling of a model network: A Gibbs-ensemble molecular dynamics study. *J. Chem. Phys.* **2000**, *112*, 5480–5487.
- [45] Lu, Z. Y.; Hentschke, R. Swelling of model polymer networks with different cross-link densities: A computer simulation study. *Phys. Rev. E* **2002**, *66*, 1–8.
- [46] Schneider, S.; Linse, P. Swelling of cross-linked polyelectrolyte gels. *Eur. Phys. J. E* **2002**, *8*, 457–460.

- [47] Schneider, S.; Linse, P. Monte Carlo Simulation of Defect-Free Cross-Linked Polyelectrolyte Gels. *J. Phys. Chem. B* **2003**, *107*, 8030–8040.
- [48] Schneider, S.; Linse, P. Discontinuous volume transitions in cross-linked polyelectrolyte gels induced by short-range attractions and strong electrostatic coupling. *Macromolecules* **2004**, *37*, 3850–3856.
- [49] Yan, Q.; de Pablo, J. J. Monte Carlo simulation of a coarse-grained model of polyelectrolyte networks. *Phys. Rev. Lett.* **2003**, *91*, 018301.
- [50] Edgecombe, S.; Linse, P. Monte Carlo simulation of polyelectrolyte gels: Effects of polydispersity and topological defects. *Macromolecules* **2007**, *40*, 3868–3875.
- [51] Binder, K. *Monte Carlo and molecular dynamics simulations in polymer science*; Oxford University Press, 1995.
- [52] Jha, P.; Zwanikken, J.; Detcheverry, F.; de Pablo, J.; Olvera de la Cruz, M. Study of volume phase transitions in polymeric nanogels by theoretically informed coarse-grained simulations. *Soft Matter* **2011**, *7*, 5965–5975.
- [53] Jiao, Y.; Torquato, S. Quantitative characterization of the microstructure and transport properties of biopolymer networks. *Phys. Biol.* **2012**, *9*, 036009.
- [54] Quesada-Pérez, M.; Ramos, J.; Forcada, J.; Martín-Molina, A. Computer simulations of thermo-sensitive microgels: Quantitative comparison with experimental swelling data. *J. Chem. Phys.* **2012**, *136*, 244903.
- [55] Košován, P.; Richter, T.; Holm, C. *Intelligent Hydrogels*; Springer, 2013; pp 205–221.
- [56] Košován, P.; Richter, T.; Holm, C. Modeling of Polyelectrolyte Gels in Equilibrium with Salt Solutions. *Macromolecules* **2015**, *48*, 7698–7708.
- [57] Kobayashi, H.; Winkler, R. G. Universal conformational properties of polymers in ionic nanogels. *Sci. Rep.* **2016**, *6*, 19836.
- [58] Schmid, A.; Dubbert, J.; Rudov, A. A.; Pedersen, J.; Lindner, P.; Karg, M.; Potemkin, I.; Richtering, W. Multi-Shell Hollow Nanogels with Responsive Shell Permeability. *Sci. Rep.* **2016**, 22736.
- [59] Adroher-Benítez, I.; Ahualli, S.; Martín-Molina, A.; Quesada-Pérez, M.; Moncho-Jordá, A. Role of steric interactions on the ionic permeation inside charged microgels: theory and simulations. *Macromolecules* **2015**, *48*, 4645–4656.
- [60] Adroher-Benítez, I.; Martín-Molina, A.; Ahualli, S.; Quesada-Pérez, M.; Odriozola, G.; Moncho-Jordá, A. Competition between excluded-volume and electrostatic interactions for nanogel swelling: effects of the counterion valence and nanogel charge. *Phys. Chem. Chem. Phys.* **2017**, *19*, 6838–6848.
- [61] Netz, P. A.; Dorfmueller, T. Computer simulation studies of diffusion in gels: Model structures. *J. Chem. Phys.* **1997**, *107*, 9221–9233.
- [62] Erbaş, A.; Olvera de la Cruz, M. Energy Conversion in Polyelectrolyte Hydrogels. *ACS Macro Lett* **2015**, *4*, 857–861.
- [63] Erbaş, A.; Olvera de la Cruz, M. Interactions between Polyelectrolyte Gel Surfaces. *Macromolecules* **2016**, *49*, 9026–9034.
- [64] Li, H.; Erbaş, A.; Zwanikken, J.; Olvera de la Cruz, M. Ionic Conductivity in Polyelectrolyte Hydrogels. *Macromolecules* **2016**, *49*, 9239–9246.
- [65] Plimpton, S. Fast Parallel Algorithms for Short-Range Molecular Dynamics. *J. Comput. Phys.* **1995**, *117*, 1–19.
- [66] Berendsen, H. J.; Postma, J. v.; van Gunsteren, W. F.; DiNola, A.; Haak, J. Molecular dynamics with coupling to an external bath. *J. Chem. Phys.* **1984**, *81*, 3684–3690.
- [67] Kienberger, F.; Pastushenko, V. P.; Kada, G.; Gruber, H. J.; Riener, C.; Schindler, H.; Hinterdorfer, P. Static and Dynamical Properties of Single Poly(Ethylene Glycol) Molecules Investigated by Force Spectroscopy. *Single Mol.* **2000**, *1*, 123–128.
- [68] Lee, H.; Venable, R. M.; Mackerell, A. D.; Pastor, R. W. Molecular dynamics studies of polyethylene oxide and polyethylene glycol: hydrodynamic radius and shape anisotropy. *Biophys. J.* **2008**, *95*, 1590–1599.
- [69] Zhang, W.; Zou, S.; Wang, C.; Zhang, X. Single polymer chain elongation of poly (N-isopropylacrylamide) and poly (acrylamide) by atomic force microscopy. *J. Phys. Chem. B* **2000**, *104*, 10258–10264.
- [70] Ahmed, Z.; Gooding, E. A.; Pimenov, K. V.; Wang, L.; Asher, S. A. UV resonance Raman determination of molecular mechanism of poly (N-isopropylacrylamide) volume phase transition. *J. Phys. Chem. B* **2009**, *113*, 4248–4256.
- [71] Kutnyanszky, E.; Embrechts, A.; Hempenius, M. A.; Vancso, G. J. Is there a molecular signature of the LCST of single PNIPAM chains as measured by AFM force spectroscopy? *Chem. Phys. Lett.* **2012**, *535*, 126–130.
- [72] Muroga, Y.; Noda, I.; Nagasawa, M. Investigation of Local Conformations of Polyelectrolytes in Aqueous Solution by Small-Angle X-ray Scattering. 2. Local Conformations of Stereoregular Poly(sodium methacrylates). *Macromolecules* **1985**, *18*, 1580–1582.
- [73] Harris, R.; Hearst, J. On polymer dynamics. *J. Chem. Phys.* **1966**, *44*, 2595–2602.
- [74] Fixman, M.; Kovac, J. Polymer conformational statistics. III. Modified Gaussian models of stiff chains. *J. Chem. Phys.* **1973**, *58*, 1564–1568.
- [75] Kierfeld, J.; Niamploy, O.; Sa-yakanit, V.; Lipowsky, R. Stretching of semiflexible polymers with elastic bonds. *Eur. Phys. J. E* **2004**, *14*, 17–34.
- [76] Rubinstein, M.; Colby, R. H. *Polymer Physics*; Oxford University Press, 2003.
- [77] Blundell, J. R.; Terentjev, E. M. Stretching Semiflexible Filaments and Their Networks. *Macromolecules* **2009**, *42*, 5388–5394.
- [78] Meng, F.; Terentjev, E. M. Theory of Semiflexible Filaments and Networks. *Polymers* **2017**, *9*, 52.
- [79] Edwards, S. F.; Freed, K. F. The entropy of a confined polymer: I. *J. Phys. A* **1969**, *2*, 145–150.
- [80] Grosberg, A. Y.; Kuznetsov, D. Quantitative theory of the globule-to-coil transition. 1. Link density distribution in a globule and its radius of gyration. *Macromolecules* **1992**, *25*, 1970–1979.
- [81] Li, Y.; Tanaka, T. Phase transitions of gels. *Annu. Rev. Mater. Sci.* **1992**, *22*, 243–277.
- [82] Mukherji, D.; Kremer, K. Coil-globule-coil transition of pnipam in aqueous methanol: Coupling all-atom simulations to semi-grand canonical coarse-grained reservoir. *Macromolecules* **2013**, *46*, 9158–9163.
- [83] Mukherji, D.; Marques, C. M.; Kremer, K. Polymer collapse in miscible good solvents is a generic phenomenon driven by preferential adsorption. *Nat. Commun.* **2014**, *5*, 4882.
- [84] Rodríguez-Ropero, F.; Hajari, T.; van der Vegt, N. F. Mechanism of polymer collapse in miscible good solvents. *J. Phys. Chem. B* **2015**, *119*, 15780–15788.

- [85] Rodríguez-Ropero, F.; van der Vegt, N. F. On the urea induced hydrophobic collapse of a water soluble polymer. Phys. Chem. Chem. Phys. **2015**, *17*, 8491–8498.
- [86] Rika, J.; Meewes, M.; Nyffenegger, R.; Binkert, T. Intermolecular and intramolecular solubilization: Collapse and expansion of a polymer chain in surfactant solutions. Phys. Rev. Lett. **1990**, *65*, 657.
- [87] Lee, L.-T.; Cabane, B. Effects of surfactants on thermally collapsed poly (N-isopropylacrylamide) macromolecules. Macromolecules **1997**, *30*, 6559–6566.
- [88] Heyda, J.; Okur, H. I.; Hladílková, J.; Rembert, K. B.; Hunn, W.; Yang, T.; Dzubiella, J.; Jungwirth, P.; Cremer, P. S. Guanidinium can both Cause and Prevent the Hydrophobic Collapse of Biomacromolecules. J. Am. Chem. Soc. **2017**, *139*, 863–870.
- [89] Moncho-Jordá, A.; Dzubiella, J. Swelling of ionic microgel particles in the presence of excluded-volume interactions: a density functional approach. Phys. Chem. Chem. Phys. **2016**, *18*, 5372–5385.
- [90] Hansing, J.; Ciemer, C.; Kim, W. K.; Zhang, X.; DeRouchey, J. E.; Netz, R. R. Nanoparticle filtering in charged hydrogels: Effects of particle size, charge asymmetry and salt concentration. Eur. Phys. J. E **2016**, *39*, 1–13.